Neuron, Volume *55*

Supplemental Data

Axon Initial Segment Kv1 Channels Control Axonal Action Potential Waveform and Synaptic Efficacy

Maarten H.P. Kole, Johannes J. Letzkus, and Greg J. Stuart

Supplemental Figure S1

Comparison in action potential (AP) properties in recordings from intact axon initial segments (AIS) versus sealed end conditions in axon 'blebs'.

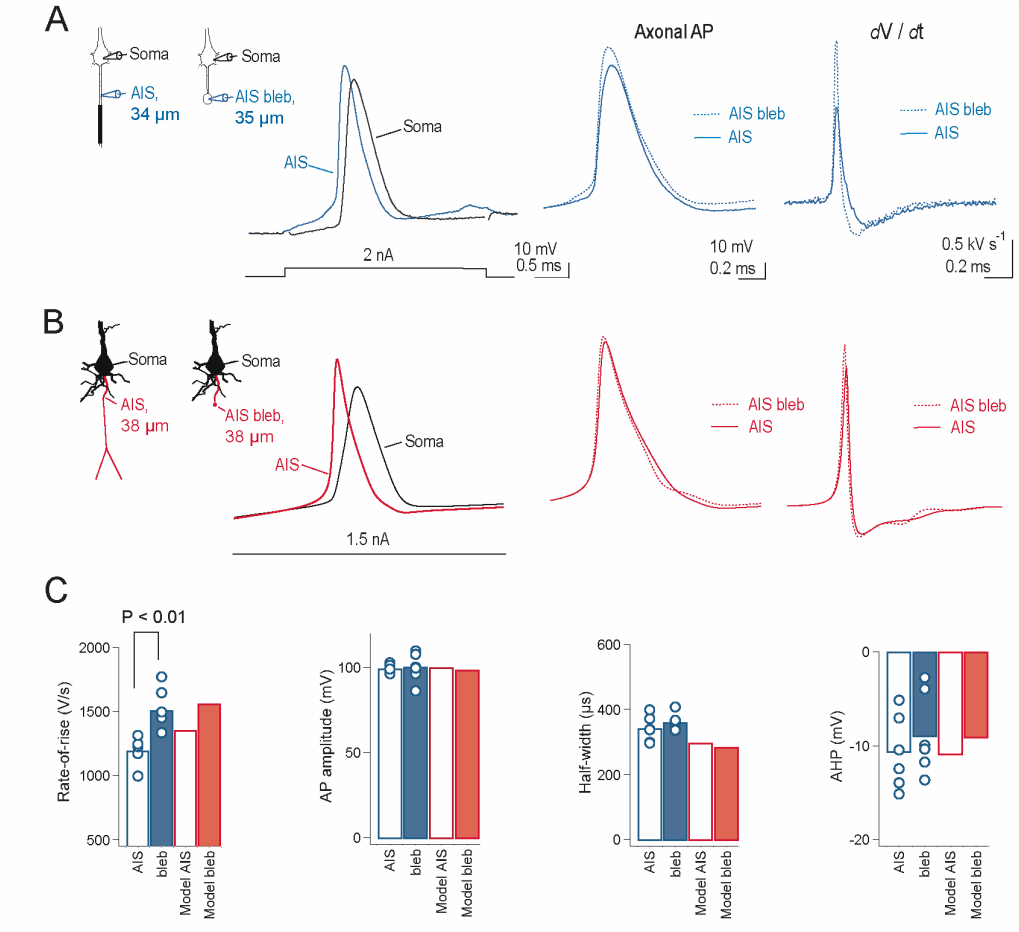

A. Left, Schematic recording configuration during simultaneous recordings from the soma (black) and AIS (blue, 34 µm from axon hillock) or from the soma (black) and an axon bleb at

a similar distance from the axon hillock (blue, 35 μm). Example traces of APs evoked by brief somatic current injection (2 nA, 3 ms) and recorded from the soma (black) and intact AIS (blue). Middle, Overlay of axonal APs from the AIS (solid) and axon bleb (dotted). Right, The derivative of the same axonal APs. Note the larger maximum AP rate-of-rise (dV/dt) in axon bleb recordings. **B**. Left, Expanded view of the model neurons used in the simulations: Soma (black) and the AIS (red; 38 μm from the hillock) or from the same soma but with an axon bleb (red; 38 μm from the hillock). The axon bleb was modelled by replacing the synthetic myelinated axon with an unmyelinated section of 4 μm length and diameter as observed experimentally (unpublished observations, Shu et al., 2006). Example traces of simulated APs at the soma (black) and intact AIS (red). APs were evoked by brief somatic current injections (1.5 nA, 5 ms). Note, APs in the model are initiated in the axon as observed experimentally. Middle, Overlay of simulated APs recorded in the AIS (solid) and axon bleb (dotted). Right, The derivative of the same simulated axonal APs. Note the larger maximum AP rate-of-rise in the model axon bleb recording. **C.** Bar graphs of experimentally recorded axonal AP properties comparing intact AIS (open blue, range: 30 – 40 μm, n = 6) and AIS axon bleb recordings (filled blue, 30 – 38 μm, n = 6) with that in simulations from the AIS (open red) and axonal blebs (filled red) at similar distances from the soma. Left, Axonal AP rate-of-rise was significantly increased in experimental axon bleb recordings (by ~315 V s^{-1}, $P < 0.01$). This increase in axonal AP rate-of-rise was mimicked in the simulations, with a ~200 V s^{-1} faster rate-of-rise in simulated axon blebs. Middle, Axonal AP amplitude and half-width were similar in experimental ($P > 0.8$, $P > 0.6$, respectively) and simulated AIS and axonal bleb recordings. Right, AHP amplitudes were not significantly different in experimental recordings from the AIS and axonal blebs ($P > 0.8$), although were slightly larger in simulations from the AIS compared to axonal blebs (< 2 mV decrease).

These data indicate that recordings from the intact AIS and axon blebs at similar distances from the axon hillock are essentially identical in all respects except that the action potential rate-of-rise is slightly greater in axon blebs. This small difference could be reproduced in compartmental models with the corresponding axonal morphology (either an intact AIS or AIS ending in a bleb, simulated as a sealed end with appropriate morphology). We conclude that axon bleb recordings are representative of recordings from the intact axon, with the proviso that there may be slight differences due to “end effects”. These data refute the notion (Naundorf et al., 2007) that axon bleb recordings are compromised by injury.

Simulation Methods

Numerical simulations were performed with NEURON 5.7 software (Hines and Carnevale, 1997) using a morphologically reconstructed neuron (Stuart and Spruston, 1998). An artificial

axon consisting of alternated cylindrical sections of myelin (length: 60 µm; diameter: 0.9 µm) and nodes (length: 1 µm; diameter: 2 µm) was connected to the end of the unmyelinated AIS (length 42 µm). The total axonal length was 2.7 mm. The passive electrical properties R_m, C_m and R_i were set to 15,000 Ωcm^2, 0.9 µF/cm^2 and 150 Ωcm, respectively, uniformly throughout axonal, somatic and dendritic compartments except for myelinated sections where C_m was set to 0.2 µF/cm^2. Active properties were incorporated using publicly available models of voltage-activated Na^+ and M-type K^+ channels (Km, Mainen and Sejnowski, 1996), non-inactivating Kv1 channels (Akemann and Knopfel, 2006) and I_h channels (Kole et al., 2006). The conductance densities (in pS µm^{-2}) were, soma: 150 Na^+, 100 Kv1 and 5 K_m, dendrites: 75 Na^+, 100 Kv1 and 5 K_m, proximal AIS (< 35 µm distance from axon hillock): 3000 Na^+, 400 Kv1 and 10 K_m, distal AIS (35 – 42 µm): 4000 Kv1 and 200 K_m, and nodes: 3000 Na^+, 100 Kv1 and 5 K_m. I_h channels were distributed in somato-dendritic sections with an exponentially increasing density with distance from the soma, but were absent in axons (Kole et al., 2006). Half-activation and half-inactivation voltage for somato-dendritic Na^+ channels was set to -21 mV and -56 mV, respectively, whereas the half-activation and half-inactivation voltage for sodium channels in the AIS and throughout the axon was set to -31 mV and -60 mV, respectively (MHP Kole; unpublished observations). Equilibrium potentials for Na^+, K^+ and I_h were set to +55 mV, –85 mV and –45 mV, respectively. The nominal simulation temperature was set at 37°C and simulations were run with 10 µs time steps.

Supplementary Figure S2

Axonal, but not somatic APs, are sensitive to low concentrations of 4-AP

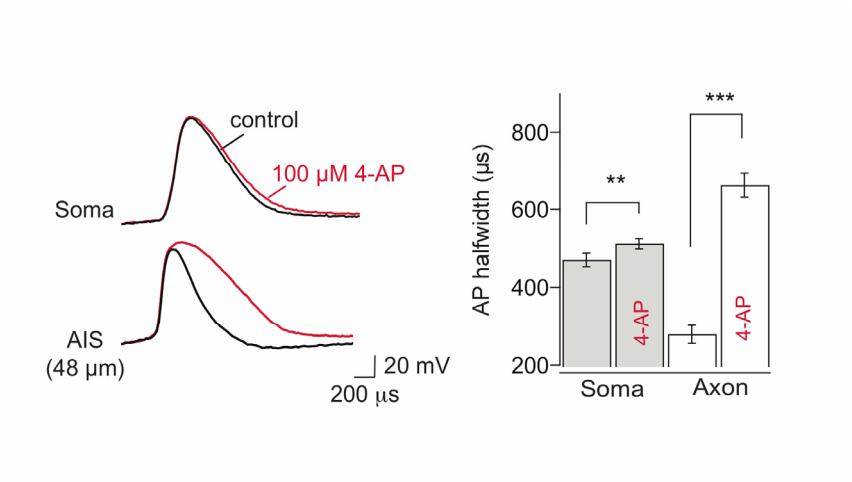

Bath application of 100 µM 4-AP, a selective blocker of K^+ channels of the Kv1 and Kv3 subfamily (Coetzee et al., 1999), led to highly localized changes in axonal AP waveform.

Figure S2 shows that 4-AP lead to a more than 2-fold increase in axonal AP half-width (control: 278 ± 23 µs; 4-AP: 661 ± 31 µs; n = 7; P < 0.001) while only slightly increasing (by 9%) somatic AP width (control: 471 ± 18 µs, 4-AP: 512 ± 13 µs; n = 7; P < 0.01). Also the afterhyperpolarization was highly significantly suppressed in the axon by ~13 mV (± 0.7 mV, n = 7; P < 0.001), but was unchanged at the soma (P > 0.05). Bath application of 4-AP also led to a slight increase in axonal AP amplitude by 12% (control: 88.2 ± 2.5 mV; 4-AP: 99.2 ± 4.1 mV; n = 7, P < 0.05). These results are identical to bath application of DTX-I (Figure 3).

Supplemental Figure S3

Spatial spread of pressure applied drug application

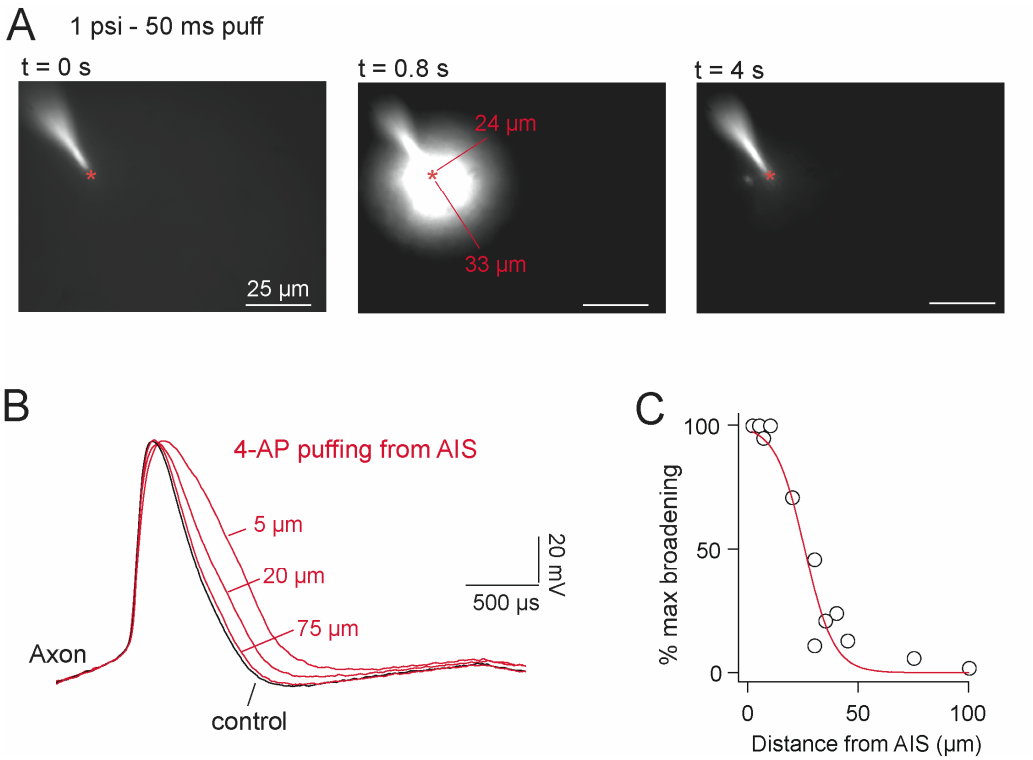

To selectively target Kv1 channels in the AIS, as in Figure 3D, we applied drugs locally through patch pipettes using a pressure application system (Picospritzer). Both the duration and pressure of the pulses were adjusted to obtain a brief ~30 µm spread of the drug as monitored by structural movements under IR-DIC. Here, we further assessed the spatial dimensions of drug spreading under these conditions. **A**. Puffs of 1 µM Alexa Fluor 488 (Molecular Probes, Australia) were applied in the slice with pressures ranging from 1 - 2 psi and with 0.05 - 2 s duration, as used experimentally. Fluorescence signals were acquired at

2.5 Hz using TILLvision (TILL Photonics GmbH, Gräfelfing Germany). Red asterisk marks the tip of the pipette. Puffs gave rise to brief circular to elliptical fluorescence changes that decayed to baseline after ~4 - 7 s. The spatial extent in these fluorescence changes was limited to ~20 to 50 µm from the tip of the application pipette depending on the pressure settings used. **B**. To further quantify the spread of pressure applications we recorded axonal and somatic APs similar to Figure 3D. Pressure applications of 100 µM 4-AP were applied at different locations either along the axon or lateral to the AIS. Left, Examples of axonal APs recorded 50 µm from the axon hillock under control conditions (black) and following local applications of 4-AP (100 µM) lateral to the AIS at the indicated locations (red). **C**. Summary plot of axonal AP half-width normalized to the maximum increase observed versus distance of local applications from the AIS (n = 12; 3 cells). Data fit with a sigmoid function with half-maximum at 25 µm. Together, these results demonstrate that drug spillover is limited to locations less than 50 µm from the application site.

Supplemental Figure S4

Relationship between DTX-I modulation and paired-pulse ratio

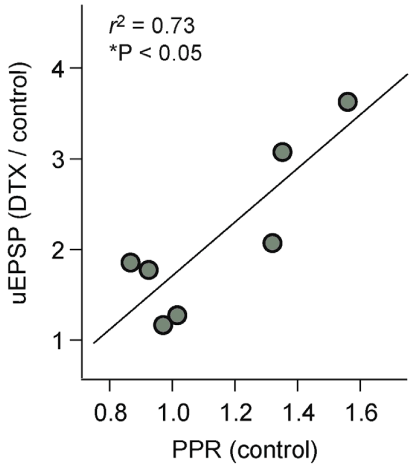

In layer 5 unitary connections there was a significant, positive correlation between the extent of uEPSP enhancement by the Kv1 channel blocker DTX-I and the paired-pulse ratio (PPR) in control (r^2 = 0.73; P < 0.05; n = 7). Given that differences in PPR are thought to reflect differences in release probability, these data indicate that DTX-I has a greater effect at synapses with low release probability (high PPR), suggesting that the release probability in cortical layer 5 axons is under the direct control of axonal Kv1 channels.

References

Akemann, W., and Knopfel, T. (2006). Interaction of Kv3 potassium channels and resurgent sodium current influences the rate of spontaneous firing of Purkinje neurons. J. Neurosci. *26*, 4602-4612.

Coetzee, W.A., Amarillo, Y., Chiu, J., Chow, A., Lau, D., McCormack, T., Moreno, H., Nadal, M.S., Ozaita, A., Pountney, D.*, et al.* (1999). Molecular diversity of K+ channels. Ann N Y Acad Sci *868*, 233-285.

Hines, M.L., and Carnevale, N.T. (1997). The NEURON simulation environment. Neural Comput. *9*, 1179-1209.

Kole, M.H.P., Hallermann, S., and Stuart, G.J. (2006). Single I_h channels in pyramidal neuron dendrites: properties, distribution, and impact on action potential output. J. Neurosci. *26*, 1677-1687.

Mainen, Z.F., and Sejnowski, T.J. (1996). Influence of dendritic structure on firing pattern in model neocortical neurons. Nature *382*, 363-366.

Naundorf, B., Wolf, F., and Volgushev, M. (2007). Neurophysiology: Hodgkin and Huxley model - still standing? (Reply). Nature *445*, E2-E3.

Shu, Y., Hasenstaub, A., Duque, A., Yu, Y., and McCormick, D.A. (2006). Modulation of intracortical synaptic potentials by presynaptic somatic membrane potential. Nature *441*, 761-765.

Stuart, G., and Spruston, N. (1998). Determinants of Voltage Attenuation in Neocortical Pyramidal Neuron Dendrites. J. Neurosci. *18*, 3501-3510.